AIAA JOURNAL
Vol. 43, No. 7, July 2005

Aspects of Low- and High-Frequency Actuation for Aerodynamic Flow Control

Ari Glezer,* Michael Amitay,† and Andrew M. Honohan‡
Georgia Institute of Technology, Atlanta, Georgia 30332-0405

Control approaches for separated flows over aerodynamic (or bluff) bodies in which the separated flow domain scales with the characteristic length of the body are distinguished by the frequency band of the actuation input. In an approach that relies on the narrowband receptivity of the separating shear layer that is coupled to the wake (shedding) instability and scales with the characteristic advection time over the separated domain, aerodynamic performance is partially restored by a Coanda-like deflection of the forced separating shear layer toward the surface. Because the instability of the unforced shear layer may already be driven by global vortex shedding, the advection of the vortices of the forced (or controlled) layer along the surface and their ultimate shedding into the near wake can couple to wake instabilities and, therefore, may result in unsteady aerodynamic forces in the controlled flow. A different control strategy that emphasizes full or partial suppression of separation by fluidic modification of the apparent aerodynamic shape of the surface relies on controlled interaction between the actuator and the crossflow on a scale that is at least an order of magnitude smaller than the relevant global length scales. A local displacement of the crossflow can alter the streamwise pressure gradient and, therefore, leads to complete or partial suppression of separation in which the actuation frequency is effectively decoupled from the global instabilities of the base flow.

I. Introduction

FLOW control strategies for external aerodynamic surfaces have mostly focused on mitigation of flow separation, which is typically precipitated by an adverse pressure gradient, for example, on a lifting surface, or by a sharp discontinuity in the flow boundary, for example, a cavity or a bluff trailing edge. Attempts to manipulate and ultimately control separation over stalled airfoils have typically relied on the narrowband receptivity of the separating flow to external actuation. The separation is simultaneously affected by two instability mechanisms, namely, a local instability of the separating shear layer and, more important, a wake instability that ultimately results in the formation and shedding of large-scale vortical structures into the wake.[1] Because the nominally time-periodic vortex shedding into the wake is accompanied by global changes in circulation, it strongly affects the evolution of the separating shear layer near the leading edge. In fact, this coupling appears to dominate the rollup of the shear layer whose natural (most unstable) frequency is typically higher than the global shedding frequency.

Because the characteristic scale of the wake is typically commensurate with the scale of the separated flow domain, earlier work on separation control over fully or partially stalled airfoils has emphasized actuation frequencies that are on the order of the shedding frequency. This corresponds to a Strouhal number $Sr_{\text{act}} = (L/U_c)/T$ of $\mathcal{O}(1)$ where the actuation period T scales with the same order as the time of flight over the separated flow domain. (L and U_c are the characteristic advection length and speed, respectively.) This approach to control separation has been applied with varying degrees of success since the early 1980s to restore aerodynamic performance of stalled airfoils and flaps.[2–5] Seifert et al.[5] argued that the actuation is most effective when the reduced frequency F^+ (which is essentially the actuation Strouhal number Sr_{act}) is $\mathcal{O}(1)$, indicating that the actuation frequency couples to and, in fact, drives the shedding in the near wake (cf. Sec. IV). Actuation at these frequencies leads to the formation of vortical structures that scale with the length of the separated flow domain, and the ensuing changes in the rate of entrainment result in a Coanda-like deflection of the separating shear layer toward the surface of the stalled airfoil, such that the layer vortices are effectively advected downstream in close proximity to the surface.[6]

The coupling (or feedback) between the time-periodic shedding of coherent vortices and the separated shear layer in the absence of actuation is intriguing because such feedback between the near-wake instabilities and the separating shear layer is even more pronounced in the presence of actuation. Although the natural frequency of the separating shear layer may be higher than the shedding frequency, the coupling between the two instabilities can result in collective interactions during the rollup. (See Ho and Huang[7] regarding the free shear layer and Unal and Rockwell[8] regarding vortex formation in the wake of bluff bodies.) More important (from the standpoint of flow control), actuation at or near the shedding frequencies can amplify the unsteady component of the global aerodynamic forces. Some of these unsteady effects were discussed in the earlier works of Amitay and Glezer[9,10] and are also evident in the numerical simulations of Wu et al.[1] (See also Sec. VI.)

A different approach to the control of flow separation on lifting surfaces emphasizes fluidic modification of the apparent aerodynamic shape of the surface upstream of separation with the objective of altering the streamwise pressure gradient to achieve complete or partial bypass (or suppression) of separation. Actuation is effected by forming a controlled interaction domain between a surface-mounted fluidic actuator, for example, a synthetic jet, and the crossflow above the surface. As demonstrated by Honohan et al.[11] and Honohan[12] on a two-dimensional cylinder, the interaction domain between a high-frequency synthetic jet and the crossflow over the surface displaces the local streamlines of the crossflow and thereby induces a virtual change in the shape of the surface (measuring roughly from two to four actuation wavelengths). The resulting change in the streamwise pressure gradient alters the evolution of the boundary layer and leads to a delay in separation. In connection with these findings, note that the formation of a small, closed separation bubble on the surface of a cylinder (at

Presented as Paper 2003-0533 at the 41st AIAA Aerospace Sciences Meeting, Reno, NV, 6–9 January 2003; received 3 January 2004; revision received 20 August 2004; accepted for publication 20 October 2004.

*Professor, Woodruff School of Mechanical Engineering. Associate Fellow AIAA.

†Research Engineer, Woodruff School of Mechanical Engineering; currently Assistant Professor, Mechanical, Aerospace and Nuclear Engineering, Rensselaer Polytechnic Institute, Troy, NY 12180. Senior Member AIAA.

‡Ph.D. Student, Woodruff School of Mechanical Engineering; currently Research Engineer, Milliken Research Corporation, Spartanburg, SC 29306.

$Re_D \approx 3.2 \times 10^5$) in the absence of flow actuation allows the boundary layer to withstand higher than normal pressure rise, and, thus, flow separation moves farther downstream, and the cylinder base pressure increases.[13] The modification of the apparent shape of aerodynamic surfaces has been exploited for controlling the evolution of both wall-bounded and free-shear flows, for example, stalled airfoils as described by Amitay et al.[14] and jet vectoring as described by Smith and Glezer,[15] respectively. Because active modification of the apparent shape of aerodynamic surfaces can potentially enable the tailoring of the pressure gradient on existing surfaces to overcome adverse pressure gradient and local separation, it may enable unconventional aerodynamic design approaches that are driven primarily by mission constraints, for example, payload, stealth, volume, etc. The compromised aerodynamic performance of such designs could potentially be augmented by the use of apparent surface modification to maintain aerodynamic performance throughout the flight envelope.[16,17]

In contrast to control approaches that rely on global manipulation of the coupled instability of the separating shear layer and the wake where the characteristic actuation wavelength scales with the affected flow domain, virtual surface shaping is based on actuation having a characteristic wavelength that is at least an order of magnitude smaller than the relevant local or global length scale of the flow. Therefore, the corresponding actuation frequencies for these two approaches are at least an order of magnitude apart, typically $\mathcal{O}(Sr_{\text{shed}})$ and $\mathcal{O}(10Sr_{\text{shed}})$ for low and high actuation frequencies, respectively. In fact, virtual surface shaping emphasizes an actuation frequency that is high enough so that the interaction between the actuator and the crossflow is essentially time invariant on the global timescale of the flow, for example, of vorticity shedding, and, therefore, is effectively decoupled from the actuation frequency in the sense that once the actuation frequency is high enough, its effect is frequency independent. This has been demonstrated in several previous works on separation control at high actuation frequencies where control authority was achieved over a broad range of Sr_{act}, including the works of Amitay and Glezer,[6] ($Sr_{\text{act}} \approx 10$), Erk[18] ($Sr_{\text{act}} \approx 100$), and, more recently, Ben-Hamou et al.[19] ($Sr_{\text{act}} = 17$–55). In fact, as was shown by Amitay and Glezer[6] and is further discussed in Sec. III, at high frequencies the actuation is effectively decoupled from the wake instability, and, therefore, the modified aerodynamic forces tend to be virtually time invariant.

The present paper focuses on illustrating some aspects of the fundamental differences in the response of a separated flow over a two-dimensional body to actuation both within the characteristic (unstable) frequencies of the separating shear layer or the near wake and well above this receptivity range. (A preliminary version of this work was also reported in an earlier paper by Glezer et al.[20]) The variation with actuation frequency of the induced aerodynamic effects on a stalled airfoil is discussed in Sec. III. Some details of the flow mechanisms that lead to these differences, including the effects of a turbulent (tripped) boundary layer were investigated in the nominally two-dimensional flow around a circular cylinder and are described in Secs. IV–VI. (The actuation wavelength is either well below or of the same order of the characteristic length scale of the body.) The cylinder flow provides direct coupling between the near-wake instability and the formation and alternate shedding of (counterrotating) large-scale vortices and the evolution of the separating shear layer. Furthermore, the choice of a cylinder minimizes higher-order effects that are associated with a specific global, for example, airfoil, geometry and has the distinct advantage that the baseline flow is extensively documented, including the evolution of the separated flow with Reynolds number.[13]

Finally, an important attribute of the control bandwidth that is enabled by high actuation frequencies is that it can also be used to augment the quasi-steady aerodynamic forces by exploiting a prescribed flow dynamics that may be compared to dynamic stall. This is accomplished by the use of temporally modulated actuation to control the rate of vorticity shedding into the wake, as demonstrated by Amitay et al.,[21] and as more recently adopted by Naim et al.[22] and Ben-Hamou et al.[19] Some of these effects are explored in the cylinder's flow and are described in Sec. VI.

II. Experimental Setup

The bulk of the experiments that are described in the present manuscript are conducted in an open-return low-speed wind tunnel having a square test section measuring 0.91 m on the side (maximum speed 50 m/s and turbulence level less than 0.15%). In the experiments described in Sec. III, the airfoil model is an unconventional airfoil that comprises a 63.2-mm-diam circular cylinder and an integral fairing based on the aft portion of a uniformly stretched NACA four-digit series symmetric airfoil, such that the combined chord is 254 mm, and the thickness ratio is 24%. (For details, see the earlier work of Amitay et al.[21]) In the experiments described in Secs. IV–VI, the model is the 63.2-mm-diam circular cylinder only.[12,23] The circular cylinder can be rotated about its spanwise axis, has a pair of adjacent spanwise jet actuators (2.5 mm apart, each 0.5 mm wide) and an azimuthal array of 47 equally spaced pressure ports. High-frequency actuation jets are generated with piezoelectric drivers in compact, shallow cavities underneath the surface of the cylinder. Low-frequency jets are generated out of the same orifices with conventional pressure speakers that are mounted on opposite ends of the cylinder cavity in the absence of the piezoelectric drivers.[23] In each frequency regime, the time-harmonic actuation waveform has a fixed (time-invariant) amplitude. The effect of a tripped (turbulent) boundary layer on the effectiveness of the actuation is assessed in a subset of the present experiments and reported in Sec. IV. Time-averaged surface pressure distributions are obtained with a differential pressure transducer. Distributions of the streamwise and cross-stream velocity components in the near wake of the airfoil and the cylinder are measured with a miniature x-wire probe mounted on a computer-controlled traversing mechanism.

III. Frequency Effects on Separation Control of a Stalled Airfoil

As noted in Sec. I, low-frequency approaches for separation control that rely on global manipulation of the instability of the separating shear layer have been investigated since the early 1980s, for example, by Ahuja and Burrin.[2] Similar or improved aerodynamic performance of stalled airfoils and bluff bodies using high actuation frequencies that are at least an order of magnitude higher than the characteristic frequencies of the separating flow or of the near wake were reported by Chang et al.,[24] Erk,[18] Smith et al.,[25] and Amitay et al.[21] However, as shown by Amitay and Glezer,[9,10] although the restored time-averaged aerodynamic forces that are attained by either control approach are nominally similar, low-frequency actuation yields instantaneous forces that have a substantial time-dependent component,[1] whereas the corresponding forces at high actuation frequencies are essentially time invariant.

The effects of the actuation frequency on the structure of the flow over a stalled, unconventional airfoil were discussed in the earlier work of Amitay and Glezer.[6] A sequence of phase-averaged smoke visualization images (each averaged over 100 realizations) is shown in Figs. 1a–1f. (The separated flow in the absence of actuation is shown for reference in Fig. 1a.) The smoke is injected in a sheet at center span and is illuminated at a given phase relative to the actuation signal using a Yag laser. In these experiments, $Re_C = 3.1 \times 10^5$, the angle of attack is $\alpha = 15$ deg, the jets angle with respect to the oncoming flow is $\gamma = 60$ deg, and their combined momentum coefficient (the two jets are driven in phase) is $C_\mu = 1.8 \times 10^{-3}$. $C_\mu = \bar{I}_j / \frac{1}{2}\rho_o U_o^2 c$, where $\bar{I}_j$ during the outstroke is

$$\bar{I}_j = \left(\frac{2}{T}\right)\rho_j b \int_0^{T/2} u_j^2(t)\,\mathrm{d}t$$

T is the actuation period; ρ_j and ρ_o are the jet and freestream fluid densities, respectively; b is the jet orifice width; c is the chord; and U_o is the freestream velocity. The jet speed at the exit plane u_j is measured with a miniature hot-wire sensor.

For low Sr_{act}, that is, $\mathcal{O}(1)$, Figs. 1b–1d, the separated shear layer is deflected toward the surface, and the passage frequency of the layer vortices is commensurate with f_{act}. These vortices persist well beyond the trailing edge of the airfoil, and it is evident that because

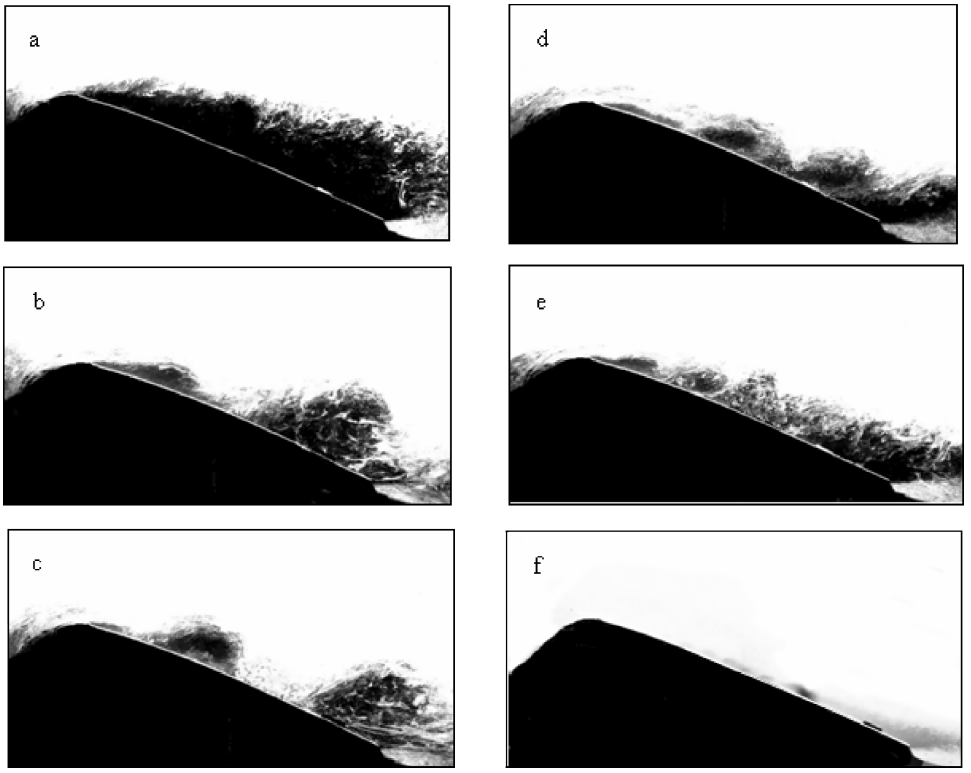

Fig. 1 Phase-averaged smoke visualization images of the flow above the surface of the airfoil ($\alpha = 15$ deg and $\gamma = 60$ deg): a) baseline and $Sr_{C\,\mathrm{act}}$ = b) 0.7, c) 1.1, d) 2.05, e) 3.3, and f) 10.

their formation frequency couples with the airfoil's natural shedding frequency ($Sr_{\mathrm{shed}} = 0.7$), they are actually enhanced as they are advected downstream, as might be predicted by stability theory. When $Sr_{C\,\mathrm{act}}$ is increased to 3.3 (Fig. 1e), the shear-layer vortices become smaller and are somewhat smeared within the domain $0.5c$ and $0.7c$ (indicating some loss of phase locking to the actuation frequency), and the flow over the surface appears to be separated beyond $0.7c$. Although the stability of the separated shear layer was not analyzed, the loss of coherence and ultimate separation in Fig. 1e suggests that as the actuation frequency increases, the actuation becomes less effective. This would indicate that the actuation frequency, which is over four times the natural shedding frequency, $Sr_{\mathrm{shed}} = 0.7$, is close to the upper end of the coupled receptivity band of the wake and the separating shear layer (cf. Sec. I) and, therefore, is not significantly amplified.

Finally, when the actuation frequency is increased to $Sr_{C\,\mathrm{act}} = 10$ (Fig. 1f), the flow appears to be fully attached to the top surface of the airfoil, and there is no evidence of organized, phase-coherent vorticity concentrations. This indicates that when the actuation frequency is high enough, the flow upstream of the stalled domain is altered such that separation is bypassed and effectively suppressed. As discussed in connection with Fig. 2, the suppression of separation at high Sr_{act} results in reduction in the width of the wake and, therefore, decoupling of the actuation from the wake instability.

The work of Amitay and Glezer[6] showed that in the presence of actuation when the flow is nominally attached to the upper surface of the airfoil, the cross-stream extent of the wake is substantially reduced and is accompanied by a reduction in the magnitudes of rms velocity fluctuations within the wake. Spectra of the streamwise velocity within the wake (Fig. 9 in Ref. 6) are reproduced in Figs. 2a–2d for the purpose of the present discussion. These power spectra are measured at $x/c = 2$ near the upper edge of the wake at a cross-stream elevation where the streamwise velocity deficit is one-half of the maximum deficit. At $Sr_{C\,\mathrm{act}} = 0.95$ (Fig. 2a) there is a strong spectral component at the actuation frequency, and the entire spectrum appears to be attenuated by approximately 3.5. As $Sr_{C\,\mathrm{act}}$ is increased to 2.05 and 3.3, the spectral peak at the actuation frequency shifts toward the decaying part of the spectrum. Note that at $Sr_{C\,\mathrm{act}} = 3.3$, the spectral peak at the actuation frequency within the

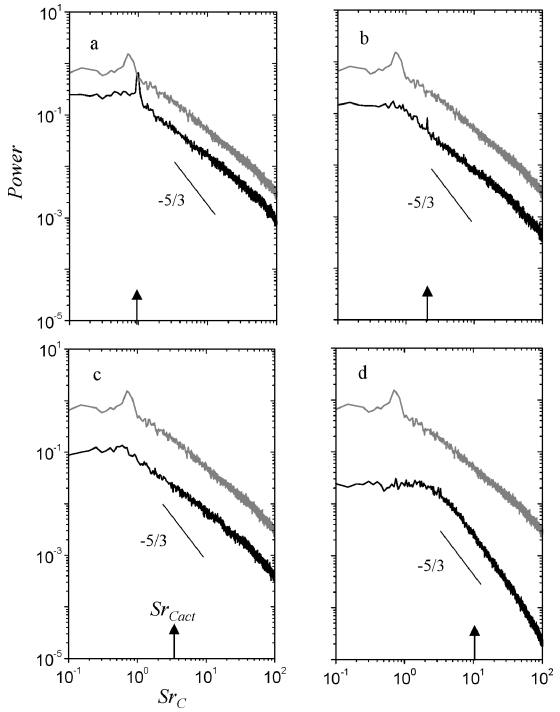

Fig. 2 Power spectra of the streamwise velocity in the wake of the airfoil: $Sr_{C\,\mathrm{act}}$ = a) 0.95, b) 2.05, c) 3.3, and d) 10; spectrum in the absence of actuation is repeated (in gray) in each frame.

wake is virtually indistinguishable from the background, indicating that even though the separated flow domain still exhibits discrete vortices at the actuation frequency, the wake is far less receptive to this frequency, and, therefore, the coupling between the separating shear layer and the wake is diminished (cf. Sec. I), and this spectral component decays. The reduction in the cross-stream extent of the separated flow domain results in nearly uniform attenuation of all spectral components by 4.5 and 7 at $Sr_{C\,\mathrm{act}} = 2$ and 3.3, respectively.

When the actuation frequency is increased to $Sr_{C\,\mathrm{act}} = 10$ (Fig. 2d), the resulting spectra are remarkably different from the corresponding spectra at the lower actuation frequencies. There is a considerably stronger attenuation (well over an order of magnitude) at both the low and high spectral ends, and the spectrum includes a distinct inertial subrange for $Sr_C > 3$ over almost two decades that also includes the actuation frequency. These findings are similar to the observations of Wiltse and Glezer,[26,27] who investigated the effects of direct excitation of the small-scale motions within free shear flows. These authors demonstrated that actuation at frequencies that are considerably higher than the natural (most amplified) frequency of the free-shear flow, which is, therefore, decoupled from the fundamental unstable frequencies of the base flow, can have a profound impact on its evolution. The actuation was applied at discrete wave numbers within the dissipation range of the base flow and resulted in significant enhancement of dissipation and attenuation of a broad range of spectral components above and below the actuation frequency, because of enhanced coupling between the small- and large-scale motions. The difference between the wake spectra in Fig. 2d is, of course, the result of the suppression of separation in the presence of actuation and the considerable reduction in the width of the wake. However, it is also evident that the increased dissipation that is affected by the high-frequency actuation leads to a substantial reduction of the turbulent kinetic energy within the wake and the appearance of a $-\frac{5}{3}$ range. The reduced power at all spectral components (compared to actuation at lower $Sr_{C\,\mathrm{act}}$) indicates that the absence of time-periodic vortex shedding into the wake and the diminished coupling to the wake instabilities at the higher actuation frequency results in lower energy transfer from the uniform stream. Note that, compared to $Sr_{C\,\mathrm{act}} = 0.95$, the high actuation frequency yields somewhat lower drag (7%) and higher lift (15%).

IV. Separated Flow over a Two-Dimensional Bluff Body

The fundamental differences in the response of a separated flow over a two-dimensional bluff body to actuation at low and high frequencies are investigated in the near field of a circular cylinder. In the absence of a well-defined separated domain, the disparate actuation wavelengths are selected to be below and above the characteristic length scale of the body, that is, $Sr_D \sim \mathcal{O}(0.1)$ and $\mathcal{O}(1)$, respectively. In what follows, the Reynolds number of the baseline flow is $Re_D = 7.55 \times 10^4$. (The Strouhal number of the natural shedding frequency is $Sr_{\mathrm{shed}} = 0.21$.) Synthetic actuation jets issue normal to the upper surface of the cylinder at an angle $\gamma = 60$ deg relative to the freestream, and the jets momentum coefficient is $C_\mu = 6 \times 10^{-4}$.

Distributions of the pressure coefficient around the cylinder for $Sr_{D\,\mathrm{act}} < 1$ and $Sr_{D\,\mathrm{act}} > 2$ are shown in Figs. 3a and 3b, respectively. The pressure distribution for the baseline flow is also shown for reference. The low frequencies include $Sr_{D\,\mathrm{act}} = 0.24$, 0.5, and 0.83, that is, $f_{\mathrm{act}} = 71$, 148, and 246 Hz, and the high frequencies include $Sr_{D\,\mathrm{act}} = 2.5$, 3.66, and 4.98, that is, $f_{\mathrm{act}} = 740$, 1088, and 1480 Hz. Actuation at the low frequencies (Fig. 3a) results in a sharp suction peak at around $\theta = 70$ deg (the same location as in the absence of actuation) the magnitude of which increases with actuation frequency. These data also show that the (time-averaged) azimuthal location of boundary-layer separation moves farther downstream when the actuation frequency increases. At $Sr_{D\,\mathrm{act}} = 0.24$ and 0.5, the flow separates at $\theta \approx 110$ deg, whereas at $Sr_{D\,\mathrm{act}} = 0.83$, the separation occurs at $\theta \approx 135$ deg. The corresponding distributions of pressure coefficient the at higher actuation frequencies ($Sr_{D\,\mathrm{act}} = 2.5$, 3.66, and 4.98; Fig. 3b) have a suction peak that is somewhat broader than those at the low frequencies, and, unlike the low frequencies, the azimuthal location of the separation appears to be invariant with frequency and occurs at $\theta \approx 135$ deg.

The variation of the coefficients of lift and pressure drag (which are computed from the pressure distributions in Figs. 3a and 3b) with the (dimensionless) actuation frequency is shown in Fig. 4. ($Sr_{D\,\mathrm{act}} = 0$ corresponds to the baseline case in the absence of actuation.) These data clearly exhibit two distinct domains that are characterized by the actuation frequency. When the actuation frequency is nominally of the same order as the natural shedding frequency,

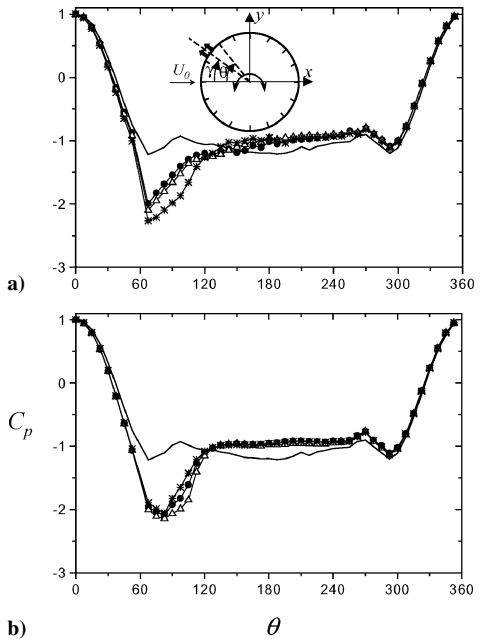

Fig. 3 Variation of the pressure coefficient with the dimensionless actuation frequency: a) $Sr_{D\,\mathrm{act}}$ = ●, 0.24; △, 0.50; and ∗, 0.83 and b) $Sr_{D\,\mathrm{act}}$ = ●, 2.50; △, 3.66; ∗, 4.98; and ——, distribution for the baseline flow.

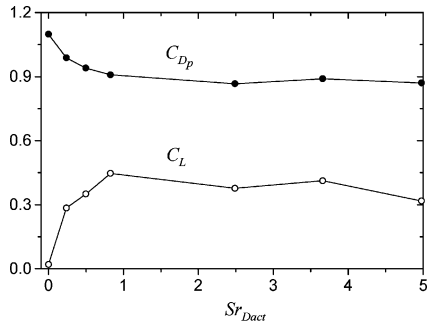

Fig. 4 Variation of the lift and the pressure drag coefficients with $Sr_{D\,\mathrm{act}}$ for $\gamma = 60$ deg.

that is, $Sr_{D\,\mathrm{act}} < 1$, the lift and pressure-drag coefficients increase and decrease, respectively, with increasing $Sr_{D\,\mathrm{act}}$. However, at actuation frequencies that are high compared to the shedding frequency, that is, $Sr_{D\,\mathrm{act}} > 1$, the lift and pressure drag coefficients appear to be almost invariant of the actuation frequency (except perhaps near $Sr_{D\,\mathrm{act}} = 5$), where nominal levels of C_L and C_{Dp} (at the present Reynolds number) are 0.4 and 0.85, respectively. This is also in qualitative agreement with the dependence of the modified aerodynamic forces on a stalled airfoil at high actuation frequencies.[6] Therefore, the absence of a local maximum at some (most amplified) frequency indicates that the actuation does not rely on varying amplification that is typical of a narrow receptivity band of shear flow instabilities (in this case, the coupled instabilities of the separated shear layer and the wake).

Because the frequency of the separated shear layer at this Reynolds number range can be on the same order as the actuation frequency ($Sr_{D\,\mathrm{act}} = 4$), it may be argued that the shear layer can be susceptible to the actuation. However, as discussed in Sec. V.A (and discussed in some detail by Hohohan[12]) vorticity maps that are measured phase locked to the actuation waveform show little or no coherent structure at the actuation frequency or its subharmonics within the separating shear layer. In addition, triple decomposition of measured turbulent fluctuations within the shear layer[12] show little contribution to the overall Reynolds stress from coherent velocity fluctuations at the actuation frequency.

The modification of the aerodynamic forces on the cylinder is accompanied by substantial changes in the structure of its wake,

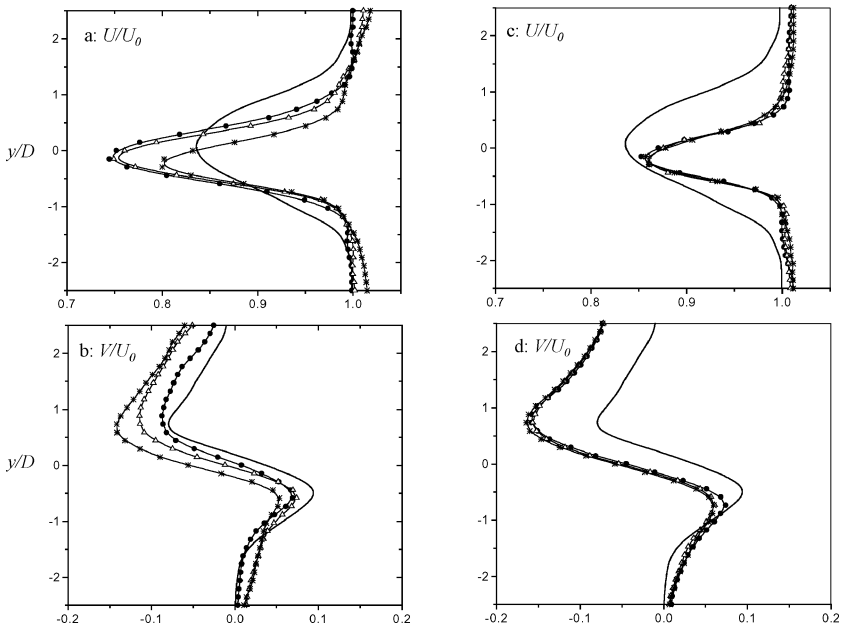

Fig. 5 Cross-stream distributions of the (normalized) time-averaged a) and c) streamwise and b) and d) cross-stream velocity components for $Sr_{D\,\mathrm{act}} \sim \mathcal{O}(0.1)$ (left) and $Sr_{D\,\mathrm{act}} \sim \mathcal{O}(1)$ (right); symbols as in Fig. 3.

which are investigated in the near wake ($x/D = 3.5$) using hot-wire anemometry. Corresponding cross-stream distributions of the time-averaged streamwise and cross-stream velocity components [$U(y/D)$ and $V(y/D)$, respectively] are shown in Figs. 5a and 5b ($Sr_{D\,\mathrm{act}} < 1$) and 5c and 5d ($Sr_{D\,\mathrm{act}} > 1$). As expected, in the absence of actuation, the cross-stream distributions of U and V are reasonably symmetric about the centerline ($y/D = 0$). When the flow is actuated within the range $Sr_{D\,\mathrm{act}} < 1$, the increase in lift and the concomitant reduction in drag are accompanied by narrowing and downward deflection of the wake, opposite to the direction of the lift. The downwash and the asymmetry (about the minimum streamwise velocity) that are induced by the actuation are also evident in the changes in distributions of the cross-stream velocity (Fig. 5b). It is remarkable that even though the wake becomes narrower, the streamwise velocity deficit is approximately 58% larger (at $Sr_{D\,\mathrm{act}} = 0.24$) than in the baseline flow, ostensibly as a result of the coupling of the actuation to the instability of the near wake and the increase in the strength of the shed vorticity concentrations. In fact, the increase in wake deficit diminishes as the actuation frequency increases, for example, 21% at $Sr_{D\,\mathrm{act}} = 0.83$.

In contrast to the frequency range $Sr_{D\,\mathrm{act}} < 1$ and in accord with the data in Fig. 4, when $Sr_{D\,\mathrm{act}} > 1$ (Figs. 5c and 5d), the distributions of U and V are almost invariant with respect to the actuation frequency. Furthermore, the wake is substantially narrower, and the velocity deficit is somewhat lower (13%) than in the baseline flow, consistent with a further increase in lift and reduction in drag (cf. Fig. 4).

The corresponding cross-stream distributions of the normalized rms velocity fluctuations u' and v' and of the Reynolds stress $u'v'$ are shown in Figs. 6a–6c ($Sr_{D\,\mathrm{act}} < 1$) and 6d–6f ($Sr_{D\,\mathrm{act}} > 1$). These data show that, in the presence of actuation, the turbulent stresses diminish at both frequency ranges but are not symmetric about the center of the wake and appear to be higher on the upper (actuated) side. This reduction is substantially higher when $Sr_{D\,\mathrm{act}} > 1$, particularly for $u'v'$, as is evident from Figs. 6c and 6f. Similar to the velocity distributions in Figs. 5c and 5d, the distributions of turbulent stresses are invariant with the actuation frequency. The lower levels of turbulent stresses at the higher actuation frequencies indicate that, in addition to global effects in terms of minimal coupling to the wake instabilities, high-frequency excitation further enhances dissipation within the separating shear layer and ostensibly in the near wake. The increase in dissipation may be the result of direct coupling of the excitation to the small-scale motions within the wake and is discussed further in Sec. V.B.

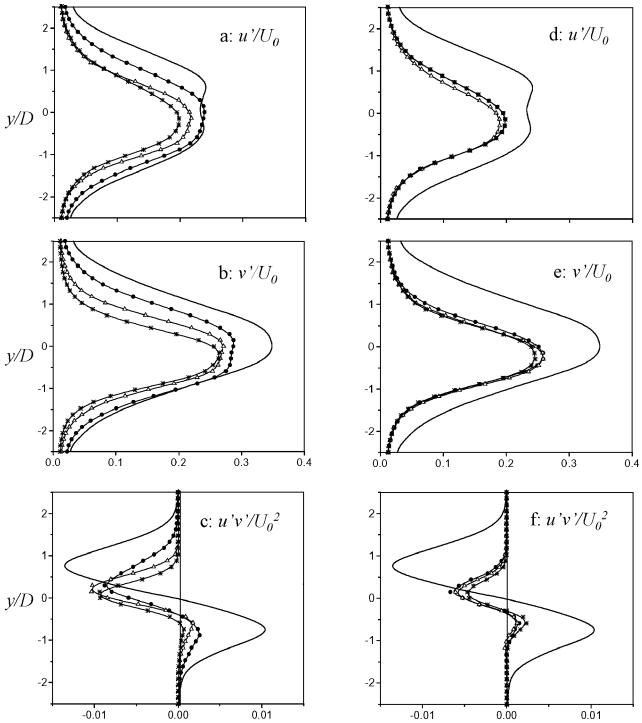

Fig. 6 Cross-stream distributions of a) and d) u', b) and d) v', and c) and e) $u'v'$ for $Sr_{D\,\mathrm{act}} \sim \mathcal{O}(0.1$ (left) and $Sr_{D\,\mathrm{act}} \sim \mathcal{O}(1)$ (right); symbols as in Fig. 3.

It might be argued that the small-scale motions that are typically associated with the high-frequency actuation induce transition to turbulence within the surface boundary layer upstream of separation. However, as shown in connection with Fig. 6 and Sec. V.B, the turbulent stresses in both the separating shear layer and the near wake, respectively, are, in fact, lower in the presence of high-frequency actuation. To assess the effects of turbulence on the actuation, the top and bottom boundary layers on the cylinder are conventionally tripped by the placement of 1-mm spanwise tube segments on the surface at $\theta = \pm 35$ deg. Similar to earlier data for a cylinders with a turbulent boundary layer, the azimuthal pressure distribution (Fig. 7)

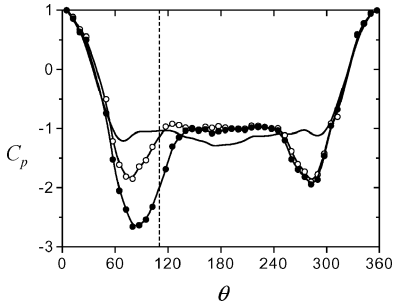

Fig. 7 Azimuthal pressure distribution $C_p(\theta)$ with a tripped boundary layer: ○, unforced; ●, actuated; and ——, smooth baseline.

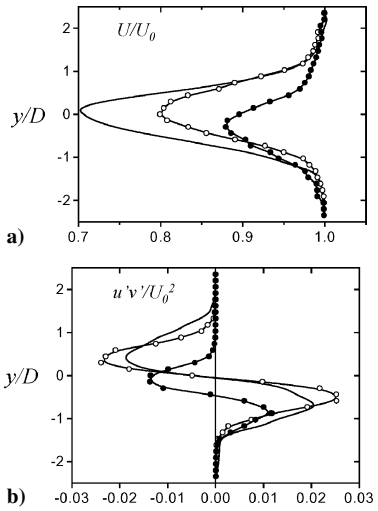

Fig. 8 Cross-stream distributions of the normalized a) streamwise velocity and b) $u'v'$: ○, baseline; ●, actuated; and ——, smooth cylinder.

in the presence of the trip (but without actuation), shows that the separation point moves from $\theta \approx 90$ to 120 deg and that the base pressure increases somewhat (indicating a decrease in pressure drag).

When the jets are activated in the presence of the trip ($\gamma = 110$ deg, $Sr_{D\,\mathrm{act}} = 2.5$), there is a substantial decrease in the static pressure both upstream (as far as $\theta \approx 30$ deg) and downstream of the actuators, and the separation point moves farther to $\theta \approx 140$ deg. Cross-stream distributions of U (measured in the presence of the trip at $x/D = 3$, Fig. 8a) show that there is a reduction in the velocity deficit of the tripped flow even in the absence of actuation. However, the deficit is further reduced when the flow is actuated and the wake is displaced downward, indicating a lift force on the cylinder. Note the effect of the jets on the distributions of $u'v'$ (Fig. 8b). Whereas $u'v'$ in the tripped flow is significantly higher than that for the smooth cylinder, the Reynolds stress in the actuated flow is substantially lower and is, in fact, even lower than $u'v'$ for the smooth cylinder.

V. Interaction of Actuation Jet with Crossflow

Some features of the nominally two-dimensional (time- and phase-averaged) interaction domain between the actuation jet and the crossflow over the surface of the cylinder are investigated using high-resolution particle image velocimetry (PIV) for both low- and high-frequency actuation. (For details, see Honohan.[12]) The measurement domain begins just upstream of the synthetic jet orifice and includes the separating shear layer on the top surface of the cylinder. These measurements were conducted in a two-dimensional (0.91×0.051 m cross section), closed-return wind tunnel with a cylinder model that is similar to the model described in Sec. II, but that has a single jet actuator. High spatial resolution (0.133 mm) is maintained over the entire domain by acquiring several sets of overlapping images (where each set includes at least 400 image pairs). The streamwise and cross-stream velocity components are computed from a cross correlation of pairs of successive images

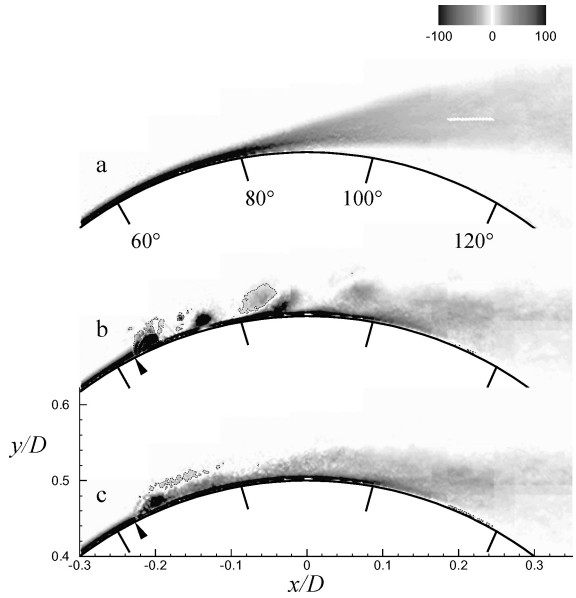

Fig. 9 Normalized vorticity $Sr_{D\,\mathrm{act}} = 4.0$: a) baseline and actuated, b) phase locked, and c) time averaged ($Re_D = 2.15 \times 10^4$, $\gamma = 63$ deg, and $C_\mu = 5.1 \times 10^{-2}$). Dashed contour corresponds to $\zeta_z = 10$.

using 32×32 pixel interrogation domains with approximately 50% overlap.

A. Interaction Domain at High Actuation Frequencies

The interaction domain between the jet and the crossflow at high actuation frequency is inferred from distributions of the spanwise vorticity (Figs. 9a–9c) that are measured along the surface of the cylinder at $Re_D = 2.15 \times 10^4$, yielding a thicker boundary layer. The time-averaged vorticity map in Fig. 9a shows that the baseline flow separates at $\theta \approx 90$ deg. Phase-averaged vorticity concentrations in the presence of actuation (Fig. 9b) show that the (counter-rotating) jet vortex pairs interact with the wall boundary layer and form a train of clockwise (CW) vortices that are advected downstream, then become weaker, and ultimately disappear within from three to four actuation wavelengths ($\lambda = 0.5U_\infty/f_{\mathrm{act}}$). These data also show that the upstream counterclockwise (CCW) jet vortex is accelerated above and around the CW vortex and rapidly weakens (within one wavelength). The time-averaged vorticity in the presence of actuation (Fig. 9c) shows a finite interaction domain that protrudes into the crossflow above the edge of the local boundary layer in the absence of actuation and that ends approximately 3–4λ downstream from the jet orifice. Some of the vorticity concentrations that are associated with the jet end up in the crossflow outside of a thinner vorticity layer near the wall and ultimately merge with the separated shear layer farther downstream. In fact, as shown later, the boundary layer downstream of the interaction domain that forms with high-frequency actuation is indeed thinner than in the baseline flow.

The interaction domain in Fig. 9c displaces the outer flow and, thereby, results in local variations in the time-averaged pressure field, which is computed from the Reynolds-averaged Navier–Stokes equations with the present PIV data. Figure 10a shows two streamlines (one each in the absence and presence of actuation) that have the same value of the stream function and that are superposed on the vorticity distribution of the actuated flow. (Note the displacement of the streamline in the presence of the actuation.) The corresponding pressure distributions along these streamlines are shown in Fig. 10b. Compared to the baseline flow, the pressure along the streamline in the presence of actuation is lower over the entire measurement domain, indicating an increase in the local velocity along the streamline due to the global changes in the flow, for example, the movement of the separation point. More significantly, within the azimuthal sector that includes the interaction domain, there is a local minimum in the pressure distribution that indicates a significant favorable pressure gradient within the crossflow above

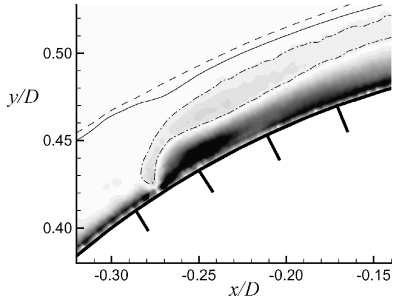

Fig. 10a Vorticity in interaction domain superimposed with streamlines having the same stream function value (ψ = 0.07): - - - -, baseline and ——, actuated. Dash–dot vorticity contour corresponds to ζ_z = 2.5.

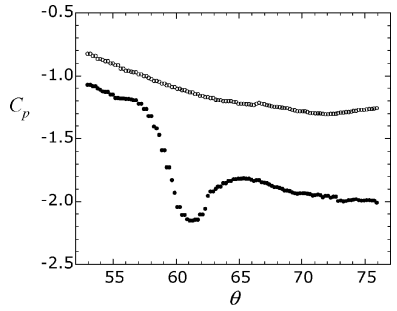

Fig. 10b Pressure coefficient along the streamlines: ○, baseline and ●, actuated.

the interaction domain. The favorable gradient is followed by a small region of weaker adverse pressure gradient, and, thereafter, there is a slight favorable pressure gradient through at least $\theta = 76$ deg. As noted in connection with Fig. 9c, it is apparent that the alteration of the streamwise pressure gradient is accompanied by a thinner, more stable boundary layer downstream of the interaction domain and a substantial delay in separation.

B. Effect of Actuation Frequency

The normalized, phase-averaged vorticity fields (with superimposed velocity profiles) are shown in Figs. 11a–11f at six equally spaced increments during a low-frequency ($Sr_{D\,\mathrm{act}} = 0.32$) actuation cycle. (Here, $\phi = 0$ deg corresponds to the synthetic jet outstroke.) Perhaps the most prominent feature of these vorticity maps is that during the low-frequency actuation cycle the separation point oscillates within a broad azimuthal sector of the cylinder surface, namely, between approximately $\theta = 87$ deg at $\phi = 0$ deg (Fig. 11a) and past $\theta = 130$ deg at $\phi = 240$ deg (Fig. 11e). The oscillation of the separation point is apparently associated with feedback between the wake and the separating shear layer and the organized, time-periodic shedding of vorticity concentrations. Therefore, the low-frequency actuation apparently results in unsteady aerodynamic forces on the cylinder and similarly on other bluff bodies or airfoils. In contrast, at a high actuation frequency ($Sr_{D\,\mathrm{act}} = 4$) that does not couple to the wake instability, the location of the separation point is virtually steady (to within one wavelength of the actuation).

Because of the long wavelength at low actuation frequencies, the flow near the jet orifice is quite different from the train of discrete vortices that are formed at high frequency (cf. Fig. 9b). The expelled actuator fluid effectively forms a wall jet that displaces and accelerates the crossflow fluid and results in a thickening of the boundary layer over much of the upper surface of the cylinder (Figs. 11b and 11c), whereas during the suction cycle the boundary layer becomes much thinner (Figs. 11e and 11f). The organized shedding of vortices at the actuation frequency begins with the formation as a small separation bubble near $x/D = 0.1$ during the suction cycle at $\phi = 240$ deg (Fig. 11e), which becomes larger and is shed at $\phi = 300$ deg (Fig. 11f).

The time-averaged, vorticity fields of the baseline flow and with low- and high-frequency actuation (Figs. 12a–12c) show that,

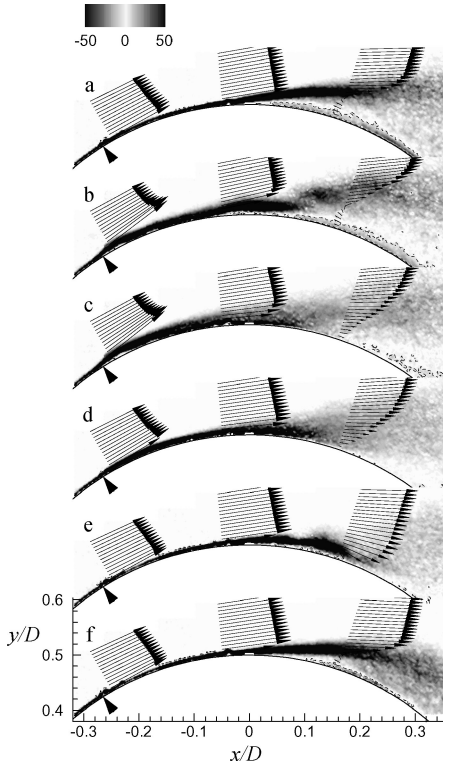

Fig. 11 Phase-averaged vorticity with superimposed cross-stream profiles of velocity vectors ($\gamma = 60$ deg, $Re_D = 7.5 \times 10^4$, $Sr_{D\,\mathrm{act}} = 0.32$, and $C_\mu = 3.8 \times 10^{-3}$): $\phi =$ a) 0, b) 60, c) 120, d) 180, e) 240, and f) 300. Dashed contour corresponds to ζ_z = 5.

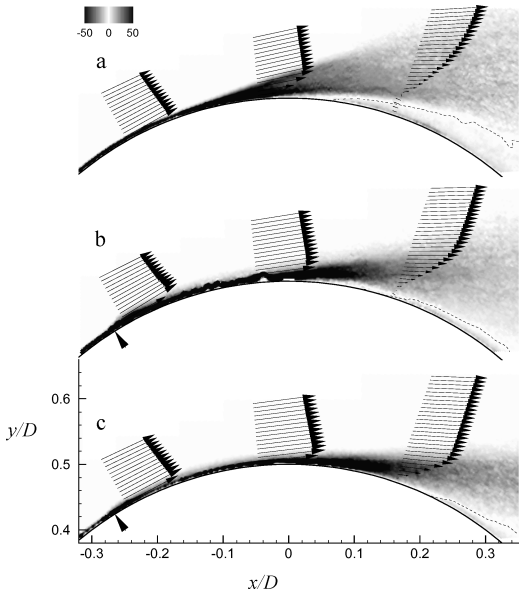

Fig. 12 Time-averaged vorticity: a) baseline, b) $Sr_{D\,\mathrm{act}} = 0.32$, and c) $Sr_{D\,\mathrm{act}} = 4.0$. Dashed contour corresponds to ζ_z = 0.

whereas boundary-layer separation is delayed at both actuation frequencies, high-frequency actuation is more effective ($\theta_{sp} = 96$ and 110 deg for $Sr_{D\,\mathrm{act}} = 0.32$ and 4.0, respectively). It is remarkable that the time-averaged separating shear layer at the low actuation frequency has approximately the same cross-stream width as in the baseline flow because of cross-stream oscillations that are evident in the phase-averaged distributions in Fig. 11. In contrast, the cross-stream width of the shear layer when the flow is forced at high frequency is considerably smaller, and its high-speed edge is almost collinear with the crossflow, indicating the absence (or at least diminution) of cross-stream oscillations.

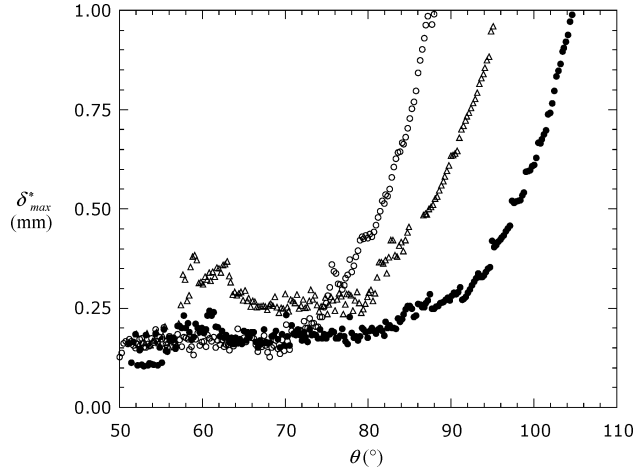

Fig. 13 Displacement thickness along the cylinder: ○, baseline; △, $Sr_{D\,act} = 0.32$; and ●, $Sr_{D\,act} = 4.0$.

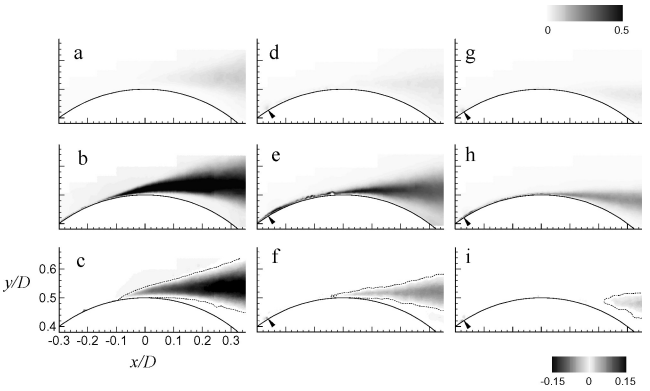

Fig. 14 Reynolds stresses: a), d), and g) $\overline{u'u'}/U_\infty^2$; b), e), and h) $\overline{v'v'}/U_\infty^2$; and c), f), and i) $\overline{u'v'}/U_\infty^2$; left column, baseline; center and right columns, $Sr_{D\,act} = 0.3$ and $Sr_{D\,act} = 4.0$, respectively; $\overline{u'v'}/U_\infty^2$ is negative within the shear layer; dashed contour in panels c, f, and i corresponds to $\overline{u'v'}/U_\infty^2 = -0.003$.

The time-averaged boundary-layer displacement thickness $\delta^*_{\max}$ (computed between the surface and the radial location of the peak tangential velocity) is used to assess the evolution of the cylinder boundary layer between the azimuthal positions of the actuator and separation (Fig. 13). These data show that the displacement of the crossflow by the ejected fluid at the low actuation frequency results in significant local increase in $\delta^*_{\max}$ (up to 100% above the baseline flow) that is followed by a nearly azimuthally invariant domain before the boundary layer begins to thicken as a precursor to separation. By comparison, the thickness of the corresponding interaction domain at the high frequency is barely measurable above $\delta^*_{\max}$ of the baseline (unforced) flow, and both remain nominally indistinguishable for $70 < \theta < 82$ deg.

As noted in connection with Fig. 6, high-frequency actuation results in a substantial reduction in the time-averaged Reynolds stresses $\overline{u'u'}$, $\overline{v'v'}$, and $\overline{u'v'}$ within the near wake. The stresses above the surface of the cylinder and within the separating shear layer at both low and high actuation frequencies are shown, along with the corresponding stresses for the baseline flow in Figs. 14a–14i. Similar to the data in Fig. 6, whereas compared to the unforced flow, the turbulent stresses in the shear layer of the forced flow are lower at both actuation frequencies, the reduction at high frequency is substantially higher. (Note, in particular, $\overline{v'v'}$ and $\overline{u'v'}$.) However, it is conjectured that the mechanisms that lead to these respective reductions are different. As shown in a number of earlier investigations on forced free-shear flows,[28] forcing the roll up of time-periodic vortices in the near wake at low actuation frequency may stunt the growth of the separating layer and limit entrainment and the evolution of small-scale motions.

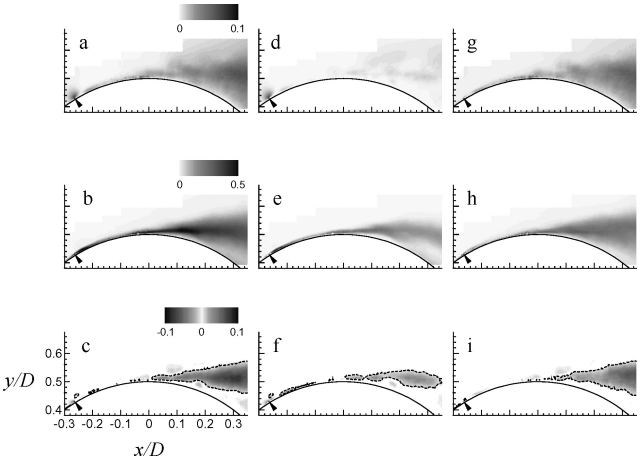

Fig. 15 Decomposition of Reynolds stresses at constant phase, $Sr_{D\,act} = 0.32$: a) $u'_r u'_r/U_\infty^2$, b) $u'_\theta u'_\theta/U_\infty^2$, c) $u'_r u'_\theta/U_\infty^2$, d) $\bar{u}'_r \bar{u}'_r/U_\infty^2$, e) $\bar{u}'_\theta \bar{u}'_\theta/U_\infty^2$, f) $\bar{u}'_r \bar{u}'_\theta/U_\infty^2$, g) $\langle \overline{\tilde{u}_r \tilde{u}_r} \rangle/U_\infty^2$, h) $\langle \overline{\tilde{u}_\theta \tilde{u}_\theta} \rangle/U_\infty^2$, and i) $\langle \overline{\tilde{u}_r \tilde{u}_\theta} \rangle/U_\infty^2$; note different contour levels for each row. Reynolds shear stress is negative within the shear layer. Dashed contour in panels c, f, and i corresponds to -0.01.

A triple decomposition of the velocity field is invoked to further elucidate the mechanisms leading to the reduction in the turbulent stresses as result of high-frequency forcing. Although fluctuations at all scales contribute to the Reynolds stress, triple decomposition of the phase-averaged velocity data into mean, coherent (phase-averaged), and random parts enables the determination of the relative contributions of the coherent and random motions. The velocity fluctuations, in polar coordinates, are separated into coherent and random components, for example, $u'_r(\boldsymbol{r}, t) = u_r(\boldsymbol{r}, t) - \bar{u}_r(\boldsymbol{r}) = \tilde{u}_r(\boldsymbol{r}, \phi) + \breve{u}_r(\boldsymbol{r}, t)$. It can be shown that the time-averaged Reynolds stresses are equal to the sum of the time-averaged correlations due to coherent fluctuations and random motion, for example, $\overline{u'_r u'_r} = \overline{(\tilde{u}_r + \breve{u}_r)(\tilde{u}_r + \breve{u}_r)} = \overline{\tilde{u}_r \tilde{u}_r} + \overline{\breve{u}_r \breve{u}_r}$, where the random velocity fluctuations are not phase locked to the data acquisition and include contributions from small-scale turbulence, phase jitter, and other unlocked large-scale motions.

As shown in Fig. 15, at low-frequency actuation ($Sr_D = 0.32$) coherent fluctuations account for a significant fraction of the total Reynolds stress, ostensibly due to the coupling of the global vortex shedding process to the actuation. As shown in a number of earlier investigations of forced free-shear flows,[28] forcing the roll up of time-periodic vortices at low actuation frequency may stunt the growth of the separating layer and limit entrainment and the evolution of small-scale motions.

In contrast to these effects of low-frequency actuation, high-frequency actuation[26] can couple directly to small-scale motions within the flow and lead to enhanced dissipation and substantial reduction in turbulent stresses. The contributions of coherent (phase-locked) and random motions for a fixed phase of the high actuation frequency ($Sr_D = 4$) are shown in Fig. 16. Whereas it is apparent that the random fluctuations within the shear layer are advected with the remnants of vorticity produced by actuation, the coherent motions do not contribute significantly to the Reynolds stresses. In other words, in the presence of high-frequency actuation, there is no significant momentum transfer within the shear layer due to coherent motions, and, thus, changes in the global flow are effected without reliance on the coupling between the actuation and instability mechanisms.

VI. Time-Modulated Actuation: Global Variation in Circulation

The coupling of both low- and high-frequency actuation approaches to global instabilities of the flow and their effects on the aerodynamic forces are investigated by measuring the changes in the circulation about the cylinder using pulsed (hat-shape) modulation of the actuation waveform. The resulting changes in circulation

are computed from phase-locked hot-wire measurements in the near wake of the cylinder. (For details, see Amitay and Glezer.[10]) The measurements typically commence ahead of the onset of the modulated actuation waveform, and the modulation is synchronized to the actuation waveform so that the leading and trailing edges of the modulating pulse coincide with zero crossing of the actuation signal.

The cross-stream time histories of the normalized spanwise vorticity distributions ($\Omega_z D/U_0$) were computed from phase-locked (relative to the modulating waveform) velocity measurements at $x/D = 3$. Figures 17a and 17b show maps of the cross-stream domains where $\Omega_z D/U_0 > 0.6$ and $\Omega_z D/U_0 < -0.6$ for $Sr_{D\,\mathrm{act}} = 0.24$ and 2.5, respectively. (Time is normalized by the actuation period T_{HFact}.) In the baseline flow (i.e., before the actuation is applied), the vorticity distribution in the wake is nominally symmetric about the wake centerline and is composed of a train of alternating vortical structures of opposite sense at the upper and lower cross-stream halves of the wake. The phase-averaged vorticity distributions ahead of the onset of the actuation should have no distinct features because there is no clear phase reference between these vortices and modulation frequency. (The presence of some details at the passage frequency of the wake vortices suggests that perhaps larger ensembles should have been acquired.) The arrivals at the measurement station of the leading and trailing edges of the modulation pulse (i.e., the onset and termination of the actuation wavetrain) are marked by strong oscillations of the wake at or near the natural shedding frequency with corresponding changes in the lift force. Ultimately, the transient changes in the vorticity flux subside, and there is a net increment in the circulation.

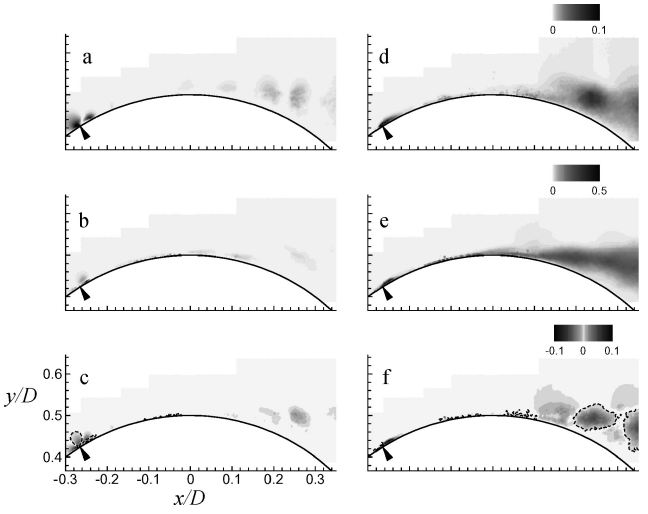

Fig. 16 Decomposition of Reynolds stresses, $Sr_{D\,\mathrm{act}} = 4$: a) $\langle \tilde{u}_r \tilde{u}_r \rangle / U_\infty^2$, b) $\langle \tilde{u}_\theta \tilde{u}_\theta \rangle / U_\infty^2$, c) $\langle \tilde{u}_r \tilde{u}_\theta \rangle / U_\infty^2$, d) $\langle \overline{u}_r \overline{u}_r \rangle / U_\infty^2$, e) $\langle \overline{u}_\theta \overline{u}_\theta \rangle / U_\infty^2$, and f) $\langle \overline{u}_r \overline{u}_\theta \rangle / U_\infty^2$; note different contour levels for each row. Dashed contour in panels c and f corresponds to −0.004.

Perhaps the most remarkable difference between the vorticity maps in Figs. 15a and 15b is the structure of the phase-averaged vorticity concentrations following the onset of actuation. At low actuation frequency (Fig. 17a), the wake is characterized by a highly regular train of phase-coherent counter-rotating vortices that occupy most (approximately 90%) of the cross-stream extent of the unforced wake. However, at the high actuation frequency (Fig. 17b) the wake is considerably narrower, and, except for three or so coherent vortices following the onset of the actuation, it is characterized by nearly incoherent CW and CCW vorticity concentrations that appear to be considerably weaker (cf. Fig. 2) than the corresponding concentrations in Fig. 17a. In both Figs. 17a and 17b, the shedding of phase-coherent vortices at the natural frequency of the cylinder is resumed following the termination of the actuation, that is, at the end of the modulation pulse.

The temporal variations in the aerodynamic force on the cylinder as a result of the actuation can be inferred from the incremental changes in the phase-averaged circulation $\Delta\Gamma$ relative to the unforced (baseline) flow (Figs. 18a and 18b). The increment is computed by time integration of the vorticity flux[10] before, during, and after the termination of the modulation. As shown in Figs. 18a and 18b, $\Delta\Gamma$ is nominally zero before the onset of actuation. Following a brief, transient, low actuation frequency (Fig. 18a) results in strong oscillations of the circulation that persist with amplitude and that are comparable to the nominal time-averaged circulation as long as the actuation is applied. These oscillations indicate, of course, that both the lift and (pressure) drag forces oscillate as well. In contrast, the transient of $\Delta\Gamma$ that is associated with the application of high-frequency actuation (Fig. 18b) decays within three cycles after the onset of the modulation pulse, and the circulation settles into a quasi-steady level (approximately 0.23) indicating that the phase-locked aerodynamic forces are also relatively time invariant. When the actuation is terminated, $\Delta\Gamma$ oscillates at nearly the natural frequency with amplitude that monotonically decays because the flow loses its phase reference with respect to the actuation.

These data underscore the fundamental difference between the low- and high-frequency actuation approaches. Whereas the low frequencies typically drive the unstable frequencies of the base flow and may result in unsteady aerodynamic forces, high actuation frequencies are deliberately selected to be well above and, therefore, decoupled from the unsteady frequencies of the base flow. Thus, the resulting phase-locked aerodynamic forces are virtually time invariant. As shown in Sec. V, high-frequency actuation is effected

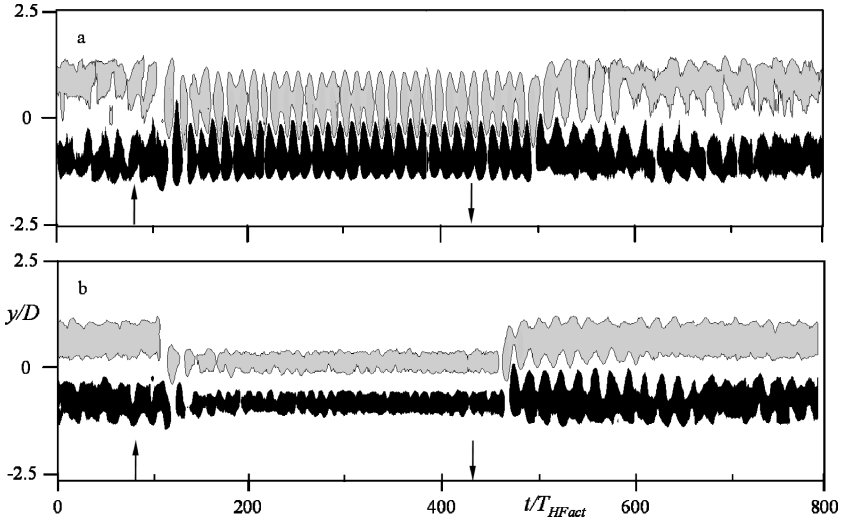

Fig. 17 Cross-stream domains in which the phase-averaged (relative to the modulating waveform) spanwise vorticity corresponds to $\Omega_z D/U_0 > 0.6$ (gray) and $\Omega_z D/U_0 < -0.6$ (black): $Sr_{D\,\mathrm{act}}$ = a) 0.24 and b) 2.5. The arrows indicate the onset and termination of actuation.

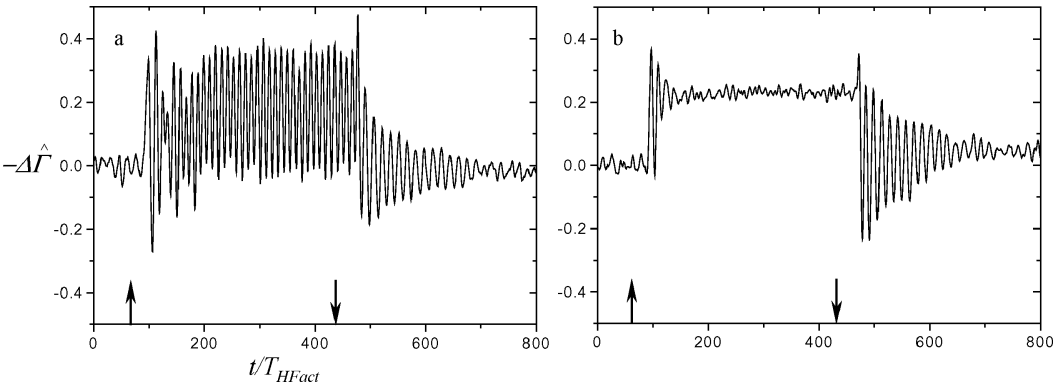

Fig. 18 Phase-averaged circulation increment for $\gamma = 60$ deg: a) $Sr_{D\,\mathrm{act}} = 0.24$ and b) $Sr_{D\,\mathrm{act}} = 2.5$.

by a change in the apparent aerodynamic shape of the body that is time invariant on a scale that is comparable to the characteristic timescale of the base flow and that is effective in attenuating (and perhaps damping) the global flow oscillations.

VII. Conclusions

Two strategies for the control of separated flows over aerodynamic surfaces are reviewed and discussed. These approaches differ substantially in terms of the coupling mechanisms between the control input and the embedding flow and are distinguished by the frequency band of the control input. In the present work, control is effected using nominally time-periodic actuation that is based on synthetic (zero net mass flux) jet actuators.

The first approach is based on the combined narrowband receptivity of the separating shear layer and the airfoil's wake to external actuation, which can affect the global flowfield by modifying the evolution of large vortical structures that are shed from the separation line into the wake. The changes in circulation that are associated with the shedding dominate the roll up of the shear layer, and, therefore, actuation at Strouhal number (or reduced frequency) of $\mathcal{O}(1)$ results in forcing of the wake instability. The actuation results in a Coanda-like deflection of the separating shear layer toward the adjacent surface, such that the layer vortices are advected downstream in close proximity to and along the surface. In this approach, the actuation period scales with the advection time over the length of the affected flow domain, and the time-periodic shedding of coherent vortices is, in fact, part of the wake. Therefore, the time-periodic shedding of vorticity concentrations into the wake of the lifting surface is accompanied by time-periodic variations of surface pressure and of the global aerodynamic forces.

A different (and more recent) approach to the control of flow separation on lifting surfaces emphasizes fluidic modification of the apparent aerodynamic shape of the surface upstream of separation, with the objective of altering the streamwise pressure gradient to achieve complete or partial bypass of separation. Actuation is effected by forming a controlled interaction domain between a surface-mounted fluidic actuator and the crossflow above the surface that may be thought of as a virtual change in the shape of the surface. In this approach, the actuation has a characteristic wavelength that is at least an order of magnitude smaller than the relevant length scale in the flow. In fact, virtual surface shaping emphasizes an actuation frequency that is high enough so that the interaction between the actuator and the crossflow is essentially time invariant on the global timescale of the flow, and, therefore, global effects, for example, vortex shedding, are effectively decoupled from the actuation frequency.

These aspects of the control approaches are investigated in the flowfield of a circular cylinder. It is shown that low-frequency actuation leads to cross-stream oscillations of the separating shear layer and strong coupling to the wake that is manifested by large azimuthal oscillations of the separation point during each actuation cycle and, therefore, translates to unsteady aerodynamic forces. When the actuation frequency is sufficiently high, the formation of a small interaction domain upstream of separation displaces the crossflow and induces a localized favorable streamwise pressure gradient that results in a thinner, more stable, boundary layer downstream of the interaction domain and a substantial delay in separation.

Finally, the coupling of both low- and high-frequency actuation approaches to global instabilities of the flow and their effects on the aerodynamic forces are investigated by measuring the changes in the circulation about the cylinder using pulsed modulation of the actuation waveform. Low-frequency actuation results in strong oscillations of the circulation and, therefore, in the aerodynamic forces. In contrast, following the application of high-frequency actuation, the circulation undergoes a brief transient and settles to a quasi-steady level, indicating that the aerodynamic forces are relatively time invariant. These findings underscore the fundamental difference between the low- and high-frequency actuation approaches, namely, that the latter is decoupled from the unsteady frequencies of the base flow and, therefore, that the derived aerodynamic forces are virtually time invariant and that global flow oscillations are attenuated and perhaps damped.

Acknowledgments

The support by the U.S. Air Force Office of Scientific Research through research grants monitored by J. M. McMichael, M. Glauser, and T. Beutner is gratefully acknowledged. The support of a NASA Langley Research Center Graduate Student Research Program Grant to A. Honohan (monitored by W. Sellers) is also gratefully acknowledged. The authors also acknowledge a number of stimulating discussions with V. Kibens (The Boeing Co., St. Louis) and D. Parekh (Georgia Tech Research Institute).

References

[1]Wu, J.-Z., Lu, X.-Y., Denny, A. G., Fan, M., and Wu, J.-M., "Post Stall Flow Control on an Airfoil by Local Unsteady Forcing," *Journal of Fluid Mechanics*, Vol. 371, 1998, pp. 21–58.

[2]Ahuja, K. H., and Burrin, R. H., "Control of Flow Separation by Sound," AIAA Paper 84-2298, Oct. 1984.

[3]Hsiao, F.-B., Liu, C.-F., and Shyu, J.-Y., "Control of Wall-Separated Flow by Internal Acoustic Excitation," *AIAA Journal*, Vol. 28, No. 8, 1990, pp. 1440–1446.

[4]Neuberger, D., and Wygnanski, I., "The Use of a Vibrating Ribbon to Delay Separation on Two Dimensional Airfoils," *Proceedings of Air Force Academy Workshop in Unsteady Separated Flow*, edited by F. J. Seiler, U.S. Air Force Academy, Colorado Springs, CO, 1987.

[5]Seifert, A., Bachar, T., Wygnanski, I., Koss, D., and Shepshelovich, M., "Oscillatory Blowing, A Tool to Delay Boundary Layer Separation," AIAA Paper 93-0440, Jan. 1993.

[6]Amitay, M., and Glezer, A., "Role of Actuation Frequency in Controlled Flow Reattachment over a Stalled Airfoil," *AIAA Journal*, Vol. 40, No. 2, 2002, pp. 209–216.

[7]Ho, C.-M., and Huang, L.-S., "Subharmonics and Vortex Merging in Mixing Layers," *Journal of Fluid Mechanics*, Vol. 119, 1982, pp. 443–473.

[8]Unal, M., and Rockwell, D., "On Vortex Formation from a Cylinder. Part 1. The Initial Instability," *Journal of Fluid Mechanics*, Vol. 190, 1988, pp. 491–512.

[9]Amitay, M., and Glezer, A., "Aerodynamic Flow Control of a Thick Airfoil Using the Synthetic Jet Actuators," American Society of Mechanical Engineers/Japan Society of Mechanical Engineering, ASME Paper FEDSM99-6922, June 1999.

[10]Amitay, M., and Glezer, A., "Controlled Transients of Flow Reattachment over Stalled Airfoils," *International Journal of Heat Transfer and Fluid Flow*, Vol. 23, Oct. 2002, pp. 690–699.

[11]Honohan, A. M., Amitay, M., and Glezer, A., "Aerodynamic Control Using Synthetic Jets," AIAA Paper 2000-2401, June 2000.

[12]Honohan, A. M., "The Interaction of Synthetic Jets with Cross Flow and the Modification of Aerodynamic Surfaces," Ph.D. Dissertation, Woodruff School of Mechanical Engineering, Georgia Inst. of Technology, Atlanta, May 2003.

[13]Roshko, A., and Fiszdon, W., "On the Persistence of Transition in the Near Wake," *Problems of Hydrodynamics and Continuum Mechanics*, Society of Industrial and Applied Mathematics, Philadelphia, 1969, pp. 606–616.

[14]Amitay, M., Smith, B. L., and Glezer, A., "Aerodynamic Flow Control Using Synthetic Jet Technology," AIAA Paper 98-0208, Jan. 1998.

[15]Smith, B. L., and Glezer, A., "Jet Vectoring Using Synthetic Jets," *Journal of Fluid Mechanics*, Vol. 458, 2002, pp. 1–34.

[16]Kondor, S., Amitay, M., Parekh, D., Fung, P., and Glezer, A., "Active Flow Control Application on a Mini Ducted Fan UAV," AIAA Paper 2001-2440, June 2001.

[17]Fung, P., and Amitay, M., "Active Flow Control Application on a Mini Ducted Fan UAV," *Journal of Aircraft*, Vol. 39, No. 4, 2002, pp. 561–571.

[18]Erk, P. P., "Separation Control on a Post-Stall Airfoil Using Acoustically Generated Perturbations," Ph.D. Dissertation, Hermann-Föttinger-Institut für Strömungsmechanik, Technische Universitat Berlin, Berlin, 1997.

[19]Ben-Hamou, E., Arad, E., and Seifert, A., "Generic Transport Aft-Body Drag Reduction Using Active Flow Control," AIAA Paper 2004-2509, June 2004.

[20]Glezer, A., Amitay, M., and Honohan, A., "Aspects of Low- and High-Frequency Aerodynamic Flow Control," AIAA Paper 2003-0533, Jan. 2003.

[21]Amitay, M., Smith, D. R., Kibens, V., Parekh, D. E., and Glezer, A., "Aerodynamic Flow Control over an Unconventional Airfoil Using Synthetic Jet Actuators," *AIAA Journal*, Vol. 39, No. 3, 2001, pp. 361–370.

[22]Naim, A., Greenblatt, D., Seifert, A., and Wygnanski, I., "Active Control of Cylinder Flow with and Without a Splitter Plate Using Piezoelectric Actuators," AIAA Paper 2002-3070, June 2002.

[23]Amitay, M., Honohan, A., Trautman, M., and Glezer, A., "Modification of the Aerodynamic Characteristics of Bluff Bodies Using Fluidic Actuators," AIAA Paper 97-2004, June 1997.

[24]Chang, R. C., Hsiao, F. B., and Shyu, R. N., "Forcing Level Effects of Internal Acoustic Excitation on the Improvement of Airfoil Performance," *Journal of Aircraft*, Vol. 29, No. 5, 1992, pp. 823–829.

[25]Smith, D. R., Amitay, M., Kibens, V., Parekh, D. E., and Glezer, A., "Modification of Lifting Body Aerodynamics by Synthetic Jet Actuators," AIAA Paper 98-0209, Jan. 1998.

[26]Wiltse, J. M., and Glezer, A., "Manipulation of Free Shear Flows Using Piezoelectric Actuators," *Journal of Fluid Mechanics*, Vol. 249, 1993, pp. 261–285.

[27]Wiltse, J. M., and Glezer, A., "Direct Excitation of Small-Scale Motions in Free Shear Flows," *Physics of Fluids*, Vol. 10, 1998, pp. 2026–2036.

[28]Oster, D., and Wygnanski, I. J., "The Forced Mixing Layer Between Parallel Streams," *Journal of Fluid Mechanics,* Vol. 123, 1982, pp. 91–130.

H. Reed
Associate Editor